PAPER

Controlling Chaotic Resonance with Extremely Local-Specific Feedback Signals

Takahiro IINUMA[†], *Student Member*, Yudai EBATO[†], *Nonmember*, Sou NOBUKAWA[†,††,†††,††††a)], *Member*,
Nobuhiko WAGATSUMA[†††††], *Nonmember*, Keiichiro INAGAKI[††††††], Hirotaka DOHO[*], *Members*,
Teruya YAMANISHI[**], *Nonmember, and* Haruhiko NISHIMURA[***], *Member*

SUMMARY Stochastic resonance is a representative phenomenon in which the degree of synchronization with a weak input signal is enhanced using additive stochastic noise. In systems with multiple chaotic attractors, the chaos–chaos intermittent behavior in attractor-merging bifurcation induces chaotic resonance, which is similar to the stochastic resonance and has high sensitivity. However, controlling chaotic resonance is difficult because it requires adjusting the internal parameters from the outside. The reduced-region-of-orbit (RRO) method, which controls the attractor-merging bifurcation using an external feedback signal, is employed to overcome this issue. However, the lower perturbation of the feedback signal requires further improvement for engineering applications. This study proposed an RRO method with more sophisticated and less perturbed feedback signals, called the double-Gaussian-filtered RRO (DG-RRO) method. The inverse sign of the map function and double Gaussian filters were used to improve the local specification, i.e., the concentration around the local maximum/minimum in the feedback signals, called the DG-RRO feedback signals. Owing to their fine local specification, these signals achieved the attractor-merging bifurcation with significantly smaller feedback perturbation than that in the conventional RRO method. Consequently, chaotic resonance was induced through weak feedback perturbation. It exhibited greater synchronization against weak input signals than that induced by the conventional RRO feedback signal and sustained the same level of response frequency range as that of the conventional RRO method. These advantages may pave the way for utilizing chaotic resonance in engineering scenarios where the stochastic resonance has been applied.

key words: *chaotic resonance, feedback control, nonlinear dynamics, and synchronization*

1. Introduction

Chaotic systems with multiple attractors in the phase space have been observed in various systems, such as nonlinear electrical circuits (e.g., Chua's circuit) and neural systems (e.g., hierarchical neural systems from the local excitatory-inhibitory neural circuit level to the macroscopic brain level [1]–[3]) (reviewed in [4], [5]). In these systems, the orbit is trapped at the nearest attractor depending on the initial conditions, whereas the attractor-merging bifurcation, which is a type of global bifurcation, causes intermittent hopping among multiple attractors, known as the chaos–chaos intermittency [4]. This system exhibits synchronization, which is a notable dynamic characteristic (reviewed in [6]).

Based on the synchronization in nonlinear systems with fluctuating barriers or thresholds, stochastic resonance is the most representative phenomenon in which the degree of synchronization with a weak input signal is maximized under the appropriate additive stochastic noise [7]–[9] (reviewed in [10]–[14]). The effect of sensitivity enhancement to weaken the external input signals has been applied in several engineering scenarios [15]–[18], particularly in neural systems [19]–[23]. However, in systems with multiple chaotic attractors, the chaos–chaos intermittent behavior in attractor-merging bifurcation causes "chaotic resonance," which is similar to stochastic resonance instead of the additive stochastic noise [6]. Chaotic resonance exhibits higher sensitivity than stochastic resonance [24]; however, it is difficult to control in several cases (reviewed in [25]). This is because adjusting the internal parameters for controlling the chaos–chaos intermittency is difficult in the outside environment, particularly in biological systems, thereby limiting the engineering applications of chaotic resonance. To overcome this difficulty, the reduced-region-of-orbit (RRO) method, which controls attractor-merging bifurcation using an external feedback signal instead of adjusting the internal parameters, was proposed [26]. The proposed method, which adjusts the profile associated with the local maximum and minimum of the nonlinear map functions of chaotic dynamics, achieves the optimal chaos–chaos intermittency for inducing chaotic resonance, thus maintaining a higher sensitivity to it [26], [27]. The RRO method has been applied to several systems, such as the discrete cubic map [26] and its assembly [28], discrete neural systems composed of excitatory–inhibitory neurons [27], [29]–[31], and Chua's

circuit [32] (reviewed in [25]).

Even in scenarios where the RRO method can be implemented using a perturbation signal lower than that of stochastic resonance, achieving a lower perturbation is still desirable. This is crucial for minimizing power consumption in the applications of chaotic resonance to electrical devices [32], [33] and ensuring minimally invasive applications to biological systems [30], [31]. In our previous preliminary study, we proposed an RRO method, called the double-Gaussian-filtered RRO (DG-RRO) method, with higher sophistication and fewer perturbed feedback signals for controlling the chaos–chaos intermittency [34]. Based on the outcome of the DG-RRO method, this study reveals the practical applicability of this model by determining whether the induced chaotic resonance maintains a higher sensitivity and wider response frequency range against the input signal than those for the conventional RRO method. The remainder of this paper is organized as follows. Section 2 reviews the chaotic resonance in systems with chaos–chaos intermittency and the RRO method for controlling chaotic resonance based on previous studies [25]. Section 3 introduces the DG-RRO method and derives the evaluation indices for the chaotic resonance induced by the DG-RRO method. Sections 4 and 5 present the results and discussions of the sensitivity and response frequency range against the input signal.

2. Related Works

2.1 Synchronization of Chaos–Chaos Intermittency in Chaotic Resonance

In a previous study [4], synchronization was induced in chaos–chaos intermittency using a weak input signal $S(t)$ in chaotic resonance within a cubic map $F(x)$, which was considered as the simplest chaotic system, as follows:

$$x(t + 1) = F(x(t)) + S(t), \qquad (1)$$

$$F(x) = (ax - x^3)\exp(-x^2/b), \qquad (2)$$

where the exponential term $F(x)$ prevents the divergent behavior of $x(t)$, and a and b are internal parameters of the map functions. Previous studies used a as the controlling parameter for chaos–chaos intermittency [4]. Figures 1(a) and (b) show instances of cubic map dynamics. Equations (1) and (2) represent the return map function of a discrete cubic map, its orbit, and the time series of $x(t)$ for the case without external signals. As shown in Fig. 1(a), under the attractor-separated conditions $F(f_{min}) < 0$ and $F(f_{max}) > 0$ (f_{min} and f_{max} correspond to the neighborhood local minima and maxima at approximately $x = 0$, respectively) [26], the orbit was trapped in the positive or negative $x(t)$ region depending on the initial condition. Contrastingly, Fig. 1(b) shows that under the attractor-merging conditions $F(f_{min}) > 0$ and $F(f_{max}) < 0$, the orbit hopped between the positive and negative $x(t)$ regions, i.e., the chaos–chaos intermittency occurred owing to the increasing absolute value of $f_{max,min}$.

Autonomous attractor switching rarely occur at the edge of the state between the chaos–chaos and non-chaos–chaos intermittencies ($F(f_{max,min}) = 0$), called the "attractor-merging bifurcation" [26]. Under this condition, applying an external input signal $S(t)$ induces attractor switching despite its weakness. Consequently, the degree of response for $S(t)$ is maximized; i.e., the chaos–chaos intermittency synchronizes with a weak $S(t)$ [4]. This sensitivity of chaotic resonance is higher than that of stochastic noise using additive stochastic noise [4], [24]. However, the application of chaotic resonance is limited in that the attractor-merging bifurcation must be adjusted using the internal parameters.

2.2 RRO Method

To overcome the difficulty of controlling the chaotic resonance, the proposed RRO method induced chaotic resonance using an external feedback signal [26]. The cubic map with a weak $S(t)$ and RRO feedback signal $Ku(t)$ is expressed as

$$x(t + 1) = F(x(t)) + S(t) + Ku(x(t)), \qquad (3)$$

$$u(x) = -(x - x_d)\exp(-(x - x_d)^2/(2\sigma_{rro}^2)), \qquad (4)$$

where K, x_d, and σ_{rro} represent the RRO feedback strength, junction of coexisting attractors (positive/negative regions), and parameter related to the influence range of feedback signals, respectively. The negative strength of K merges the attractor with the bifurcation [27]. In a previous study, the parameters for x_d and σ_{rro} were set as $x_d = 0$ and $\sigma_{rro} = 0.6$, respectively [26]. Figure 1(c) shows the return map function of the discrete cubic map using the RRO feedback signal given in Eqs. (3) and (4). Instead of increasing the a value, the RRO feedback signal $K = -0.3$ induced the attractor-merging conditions $F(f_{min}) + Ku(f_{min}) > 0$ and $F(f_{max}) + Ku(f_{max}) < 0$, i.e., the chaos–chaos intermittency. Therefore, high-sensitive chaotic resonance can be generated using attractor-merging bifurcation induced by the RRO feedback signal [27].

3. Material and Methods

3.1 Discrete Cubic Map and the DG-RRO Method

Based on the parameter set used in our previous study ($\sigma_{rro} = 0.6, x_d = 0$), the RRO feedback signal expressed in Eq. (4) comprises a linear function $-(x - x_d)$ that adjusts the local maxima and minima of the map function F and a single Gaussian function around the attractor dividing point x_d, as shown in the upper part of Fig. 2 [26]. However, the local specification around $x = x_{min,max}$ ($x_{min,max}$: $f_{min,max} = f(x_{min,max})$) in the feedback signal, i.e., degree to which the feedback signal rapidly approaches to zero with increasing the distance from $x = x_{min,max}$, can be improved.

To address this issue, we used the sign reversal function $-F(x)$ and double Gaussian functions at $x = x_{min,max}$, i.e., the "DG-RRO feedback signals $g(x)$." This signal expressed the discrete cubic map as follows:

$$x(t + 1) = F(x(t)) + S(t) + Kg(x(t)), \qquad (5)$$
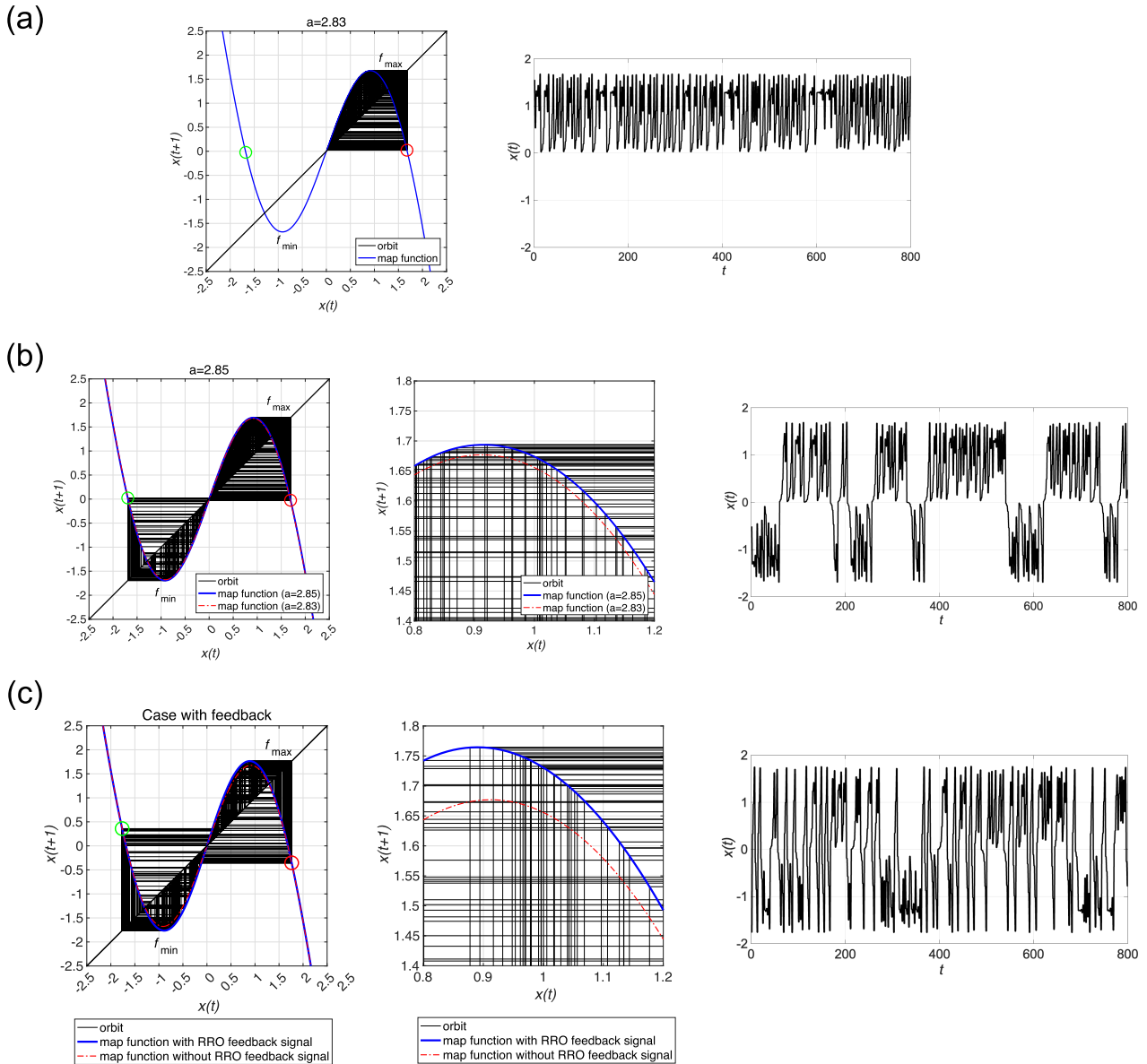
Fig. 1 (a) Return map function of a discrete cubic map expressed in Eqs. (1) and (2) and its orbit (left parts) and the corresponding time series of $x(t)$ (right parts) for the case without external signals $S(t) = 0$, $K = 0$ under the attractor-separated condition $F(f_{\min}) < 0$ (green open circle) and $F(f_{\max}) > 0$ (red open circle) at $a = 2.83$. The initial condition $x(0)$ is set to a positive value, and $f_{\min}$ and $f_{\max}$ correspond to the local minima and maxima near $x = 0$, respectively. (b) Return map function and its orbit (left part) and the corresponding time series $x(t)$ (right part) under the attractor-merging conditions $F(f_{\min}) > 0$ (green open circle) and $F(f_{\max}) < 0$ (red open circle) at $a = 2.85$. (Center part) Magnified region around the local maximum of the map function F. (c) Return map function of a discrete cubic map expressed in Eqs. (3) and (4), and its orbit (left parts) and the corresponding time series of $x(t)$ (right parts) for the RRO feedback signal ($K = -0.3$), which is increased instead of a ($a = 2.83$) in the absence of the input signal $S(t) = 0$. The initial condition $x(0)$ is set to a positive value. The center part represents the attractor-merging condition $F(f_{\min}) + K(f_{\min}) > 0$ (green open circle) and $F(f_{\max}) + K(f_{\max}) < 0$ (red open circle). (Center part) Magnified region around the local maximum of the map function F.

$$g(x) = -F(x)(\exp(-(x - x_{\min})^2/(2\sigma_{\mathrm{dg}}^2))$$
$$+ \exp(-(x - x_{\max})^2/(2\sigma_{\mathrm{dg}}^2)), \qquad (6)$$

where σ_{dg} is a parameter related to the influence range of the feedback signal. We set $\sigma_{\mathrm{dg}} = \sigma_{\mathrm{rro}}/2$ corresponding to σ_{rro}. The lower part of Fig. 2 shows the $g(x)$ profile.

Compared with the RRO feedback signal, $g(x)$ converged more rapidly to zero, except at $x = x_{\min,\max}$, i.e., the DG-RRO method achieved a higher local specification near the local minima/maxima.

To evaluate the signal response in these dynamics, a weak signal $S(t)$ was applied. In this study, the weak sinu-
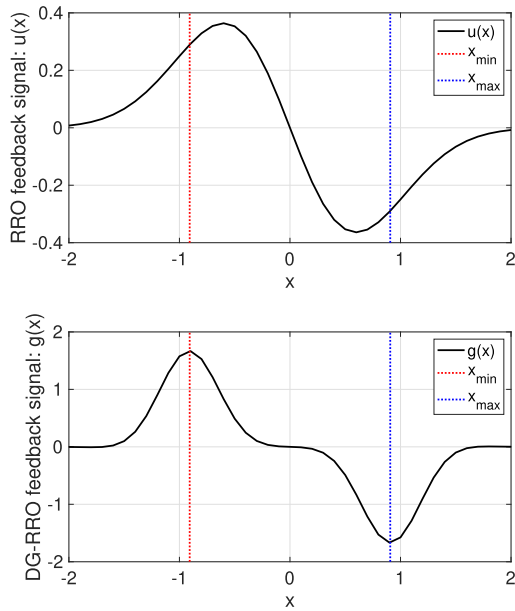
Fig. 2 (Upper part) The RRO feedback signal $u(x)$ expressed in Eq. (4) and local minima (x_{min})/maxima (x_{max}) for the map function $F(x)$ expressed in Eq. (2). (Lower part) The DG-RRO feedback signal $g(x)$ expressed in Eq. (6). Compared with the RRO feedback signal, $g(x)$ converges to zero more rapidly while leaving $x = x_{min,max}$ (called the local specification), i.e., the DG-RRO method achieves a higher local specification around the local minima/maxima.

soidal signal applied was $S(t) = A_s \sin \Omega t$ with strength A_s and frequency Ω.

3.2 Evaluation Indices

3.2.1 Attractor-Merging Bifurcation

To capture attractor-merging bifurcation, we used a bifurcation diagram of $x(t)$, and $F(f_{max,min}) + Ku(f_{max,min}) = 0$ and $F(f_{max,min}) + Kg(f_{max,min}) = 0$ for the RRO and DG-RRO feedback signals, respectively [26].

3.2.2 Perturbation in the Feedback Signals

The amount of perturbation in the applied feedback signal is evaluated as follows: $\Theta = < (Ku(x(t)))^2 >$ for the RRO feedback signal and $\Theta = < (Kg(x(t)))^2 >$ for the DG-RRO feedback signal, where $< \cdot >$ is the average in t. To evaluate the instantaneous maximum perturbation in feedback signals, we investigated the maximum perturbation of $(Ku(x))^2$ and $(Kg(x))^2$ during the evaluation duration, denoted as Θ_{max}. These values were assessed in 10 trials using different initial conditions of $x(0)$.

3.2.3 Mutual Correlation between the Chaos–Chaos Intermittency and Input Signal

To quantify the synchronization between the chaos–chaos intermittency of $x(t)$ and $S(t)$, their mutual correlation was evaluated by considering the time delay τ as follows:

$$C(\tau) = \frac{C_{sx}(\tau)}{\sqrt{C_{ss} C_{xx}}}, \tag{7}$$

$$C_{sx}(\tau) = \langle (S(t + \tau) - \langle S \rangle)(X(t) - \langle X \rangle) \rangle, \tag{8}$$

$$C_{ss} = \langle (S(t) - \langle S \rangle)^2 \rangle, \tag{9}$$

$$C_{xx} = \langle (X(t) - \langle X \rangle)^2 \rangle, \tag{10}$$

where $\langle \cdot \rangle$ denotes the average t; and X represents the binarized $x(t)$ value, i.e., $X(t) = 1$ when $x(t) \geq 0$ and $X(t) = -1$ in $x(t) < 0$. These values focus on the chaos–chaos intermittency instead of the intra-each-region ($x(t) \geq 0$ or $x(t) < 0$). We set τ to $\max_\tau C(\tau)$ for each time series of $x(t)$ and evaluated $\max_\tau C(\tau)$ in 10 trials using different initial conditions of $x(0)$. To compare the degree of synchronization between the RRO and DG-RRO methods, t-test was performed for the trials at specific internal parameters and feedback strength of K. The statistical significance was set to $p < 0.05$.

4. Results

4.1 Controlling Attractor-Merging Bifurcation Using Feedback Signals

The effect of DG-RRO feedback signals on inducing attractor-merging was compared with that of the conventional RRO feedback signals. Figure 3 shows that $x(t)$ is a function of the strength of the feedback signal K. It displays the bifurcation diagram, amount of perturbation Θ, and maximum perturbation Θ_{max}, and the following conditions for attractor-merging bifurcation: $F(f_{max,min}) + Kg(f_{max,min})$ for the DG-RRO feedback signal and $F(f_{max,min}) + Ku(f_{max,min})$ for the RRO feedback signal. In both cases, the separated attractors were merged using the negative feedback signals at $K \approx -0.0065$ and $K \approx -0.039$ for the DG-RRO and RRO feedback signals, respectively, satisfying $F(f_{max,min}) + Kg(f_{max,min}) = F(f_{max,min}) + Ku(f_{max,min}) = 0$. K_{am} denotes these K strengths. The amount of perturbation Θ and maximum perturbation Θ_{max} of the DG-RRO feedback signal were significantly smaller than those of the RRO feedback signal (one- and two-third for Θ and Θ_{max}, respectively). To verify whether this tendency is sustained under different internal parameter a settings, Fig. 4 shows the K_{am} dependence on a using the RRO and DG-RRO methods and the amount of perturbation Θ at the corresponding feedback strength $K = K_{am}$. Consequently, the DG-RRO method achieved attractor-merging bifurcation with significantly fewer perturbations in the evaluated range of a.

4.2 Inducing Chaotic Resonance

Based on the effect of induced attractor-merging, we evaluated whether the chaotic resonance can be controlled. Figure 5 shows the mutual correlation $\max_\tau C(\tau)$ between the chaos–chaos intermittency of $x(t)$ and the input signal $S(t) = A_s \sin \Omega t$, considering the time delay τ as a function of K and a when the RRO and DG-RRO feedback signals are applied. In both cases, $\max_\tau C(\tau)$ exhibits a unimodal maximum peak as K varies, i.e., chaotic resonance is induced
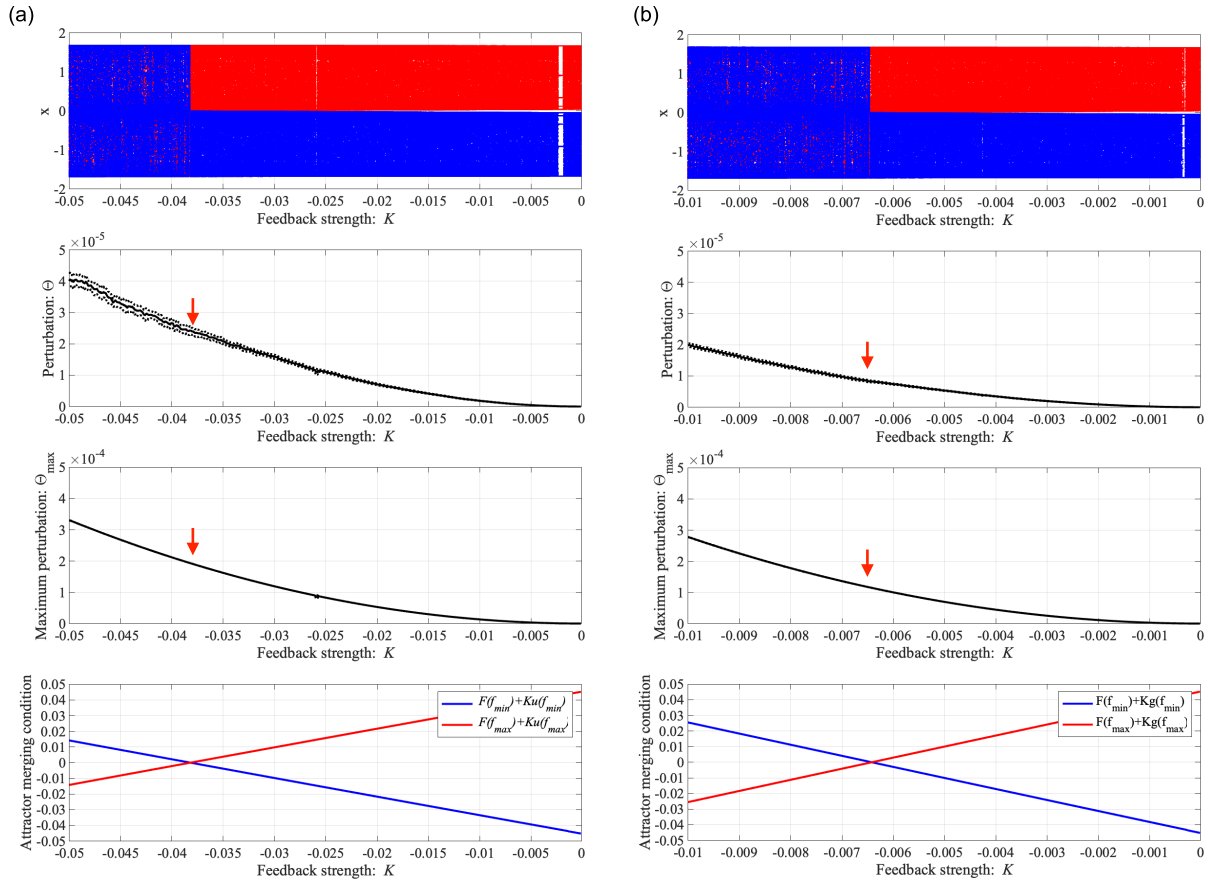
Fig. 3 $x(t)$ is a function of the strength of the feedback signals K. (a) Case for controlling by RRO feedback signal. (b) Case for controlling by the DG-RRO feedback signal. (1st line) Bifurcation diagram of $x(t)$ (blue and red dots denote the negative and positive initial values, respectively). (2nd line) Amount of perturbation Θ (red arrow corresponds to K for attractor-merging bifurcation, which is denoted as K_{am}. Solid and dotted lines represent the mean and standard deviation of the results of 10 trials with different initial values of $x(0)$, respectively). (3rd line) Maximum perturbation Θ_{max} in the evaluation duration (red arrow corresponds to K_{am}. Solid and dotted lines represent the mean and standard deviation of the results, respectively). (4th line) Condition for attractor-merging bifurcation $F(f_{\text{max,min}}) + Ku(f_{\text{max,min}})$ for the RRO feedback signal and $F(f_{\text{max,min}}) + Kg(f_{\text{max,min}})$ for the DG-RRO feedback signal. In both cases, the separated attractors are merged using negative feedback signals. The DG-RRO feedback signal can induce attractor-merging bifurcation via a smaller perturbation ($a = 2.82$, $b = 10$, $\sigma_{\text{rro}} = 0.6$, $\sigma_{\text{dg}} = 0.3$).

under the attractor-merging condition, as shown in Fig. 3.

The sensitivities of the RRO and DG-RRO methods were evaluated. Figure 6(a) shows the signal strength A_s and K dependency of mutual correlation $\max_\tau C(\tau)$ at $a = 2.82$ (corresponding to the same internal a value shown in Fig. 3). Consequently, in the attractor-merging bifurcation ($K = -0.038$ for the RRO method and $K = -0.0064$ for the DG-RRO method), a high value of $\max_\tau C(\tau)$ was sustained even for the weak input $A_s \approx 10^{-4}$. To compare the degrees of synchronization, Fig. 6(b) shows the $\max_\tau C(\tau)$ values for each trial in both cases using the RRO and DG-RRO feedback signals in $A_s = 10^{-3}, 10^{-4}$. Consequently, the values of $\max_\tau C(\tau)$ were the same in the two methods ($t = 0.956, p = 0.351$) at $A_s = 10^{-3}$. However, for a smaller signal strength $A_s = 10^{-4}$, a significantly larger $\max_\tau C(\tau)$ was achieved using the DG-RRO method than that achieved using the RRO method ($t = 2.12, p = 0.047$).

The input frequency range, in which a high degree of synchronization was sustained between the RRO and DG-RRO methods, was compared. Figure 7 shows the signal frequency Ω and K dependency of the mutual correlation $\max_\tau C(\tau)$ at $a = 2.82$ (corresponding to the same a value shown in Fig. 3). In both cases, a high value of $\max_\tau C(\tau)$ distributes in the same frequency range $0.001 \lesssim \Omega \lesssim 0.03$ under the attractor-merging condition ($K = -0.038$ for the RRO method and $K = -0.0064$ for the DG-RRO method). Therefore, the input frequency range of the chaotic resonance induced by the DG-RRO method was maintained at the same level as that of the conventional RRO method.

5. Discussion and Conclusions

This study developed an extremely weak DG-RRO feedback signal to control the attractor-merging bifurcation. This signal was compared to the feedback signal induced using the conventional RRO methods. The DG-RRO feedback signal
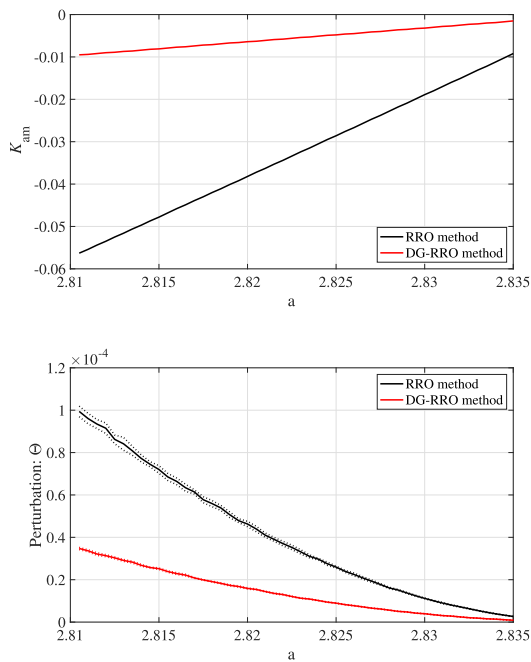
Fig. 4 (Top) Feedback strengths to induce attractor-merging bifurcation, satisfying $F(f_{\text{max,min}}) + Ku(f_{\text{max,min}}) = 0$ (RRO method) and $F(f_{\text{max,min}}) + Kg(f_{\text{max,min}}) = 0$ (DG-RRO method): K_{am} as function of a for the RRO and DG-RRO methods. (Bottom) Amount of perturbation Θ at $K = K_{\text{am}}$. Solid and dotted lines represent the mean and standard deviation of the results of 10 trials with different initial values of $x(0)$, respectively. The DG-RRO method achieves attractor-merging bifurcation using significantly fewer perturbations ($b = 10$, $\sigma_{\text{rro}} = 0.6$, $\sigma_{\text{dg}} = 0.3$).
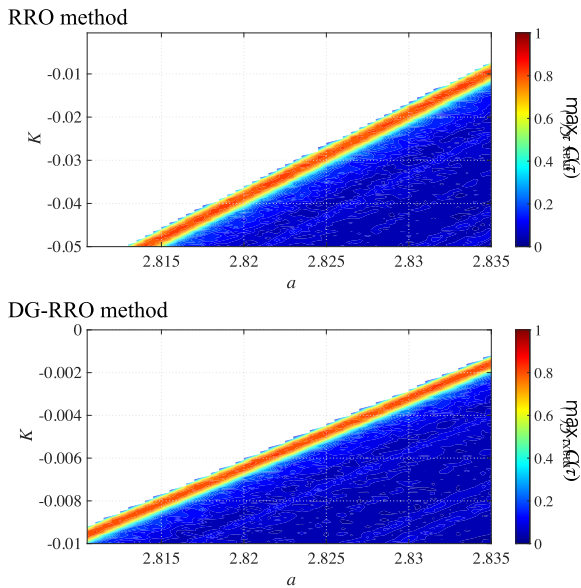
Fig. 5 K and a dependency of the mutual correlation $\max_\tau C(\tau)$ between the chaos–chaos intermittency of $x(t)$ and the input signal $S(t) = A_s \sin \Omega t$, considering the time delay τ. White region corresponds to no-chaos–chaos intermittency. The $\max_\tau C(\tau)$ values are averaged from the results of the 10 trials with different initial values of $x(0)$. (Upper part) Applying the RRO feedback signal. (Lower part) Applying the DG-RRO feedback signal. In both cases, $\max_\tau C(\tau)$ exhibits a unimodal maximum peak as K varies, i.e., chaotic resonance is induced under the attractor-merging condition, as shown in Fig. 3 ($b = 10$, $\sigma_{\text{rro}} = 0.6$, $\sigma_{\text{dg}} = 0.3$, $A_s = 0.001$, $\Omega = 0.005$).
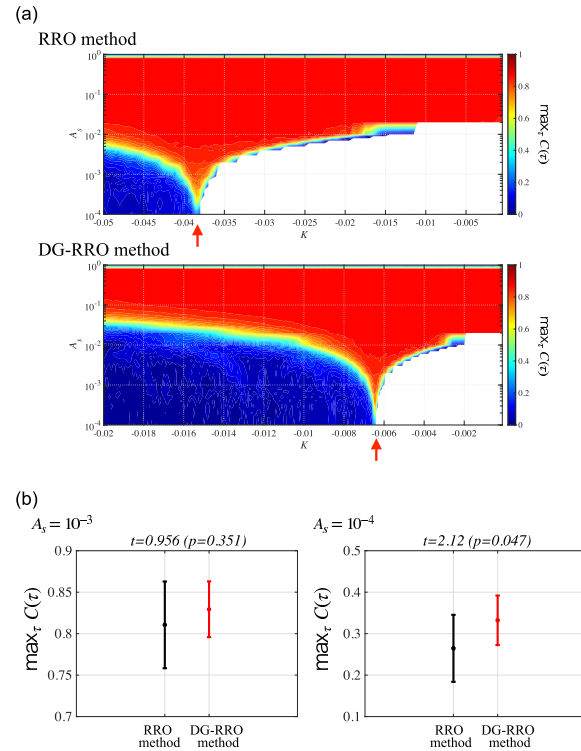
Fig. 6 (a) A_s and K dependency of $\max_\tau C(\tau)$ between the chaos–chaos intermittency of $x(t)$ and the input signal $S(t) = A_s \sin \Omega t$, considering the time delay τ. White region represents the no-chaos–chaos intermittency. The $\max_\tau C(\tau)$ values are averaged from the results of the 10 trials with different initial values of $x(0)$. (Upper part) Applying the RRO feedback signal. (Lower part) Applying the DG-RRO feedback signal. In both cases, a high value of $\max_\tau C(\tau)$ is sustained using a weak input $A_s \approx 10^{-4}$ under the attractor-merging condition ($K = -0.038$ for the RRO method and $K = -0.0064$ for the DG-RRO method, as represented by the red arrows). (b) (Left part) $\max_\tau C(\tau)$ values for each trial in both cases using the RRO and DG-RRO feedback signals at $A_s = 10^{-3}$. (Right part) $\max_\tau C(\tau)$ values for each trial in both cases using the RRO and DG-RRO feedback signals at $A_s = 10^{-4}$. The dot and error bars represent the mean and standard deviation of the results of the 10 trials, respectively ($a = 2.82$, $b = 10$, $\sigma_{\text{rro}} = 0.6$, $\sigma_{\text{dg}} = 0.3$, $\Omega = 0.005$).

was determined using the inverse sign of the map function and double Gaussian filters around the local maxima and minima. Owing to its fine local specification, the DG-RRO feedback signal achieved the attractor-merging bifurcation using a significantly smaller feedback perturbation than that of the conventional RRO method, thereby inducing the chaotic resonance. This resonance exhibited a higher degree of synchronization against weak input signals than that of the conventional RRO feedback signal, sustaining the same level of the response frequency range as that of the conventional RRO method.

The DG-RRO feedback signals achieved local specifications around the local maxima and minima of the map function (Fig. 2). Therefore, these signals in other regions with local maxima/minima $x_{\text{max,min}}$ were significantly smaller than the RRO feedback signals. This decreased the total and instantaneous values of the perturbation of the feedback signal, corresponding to Θ and Θ_{max}, respectively. Conse-
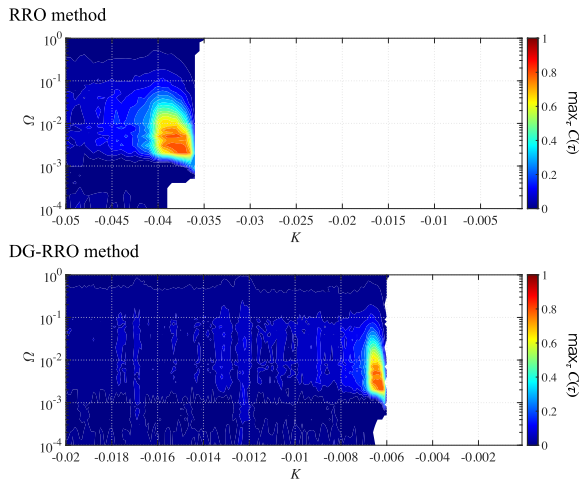
RRO method

DG-RRO method

Fig. 7 Ω and K dependency of $\max_\tau C(\tau)$ between the chaos–chaos intermittency of $x(t)$ and the input signal $S(t) = A_s \sin \Omega t$, considering the time delay τ. White region represents the no-chaos–chaos intermittency. The $\max_\tau C(\tau)$ values are averaged from the results of 10 trial with different initial values of $x(0)$. (Upper part) Applying the RRO feedback signal. (Lower part) Applying DG-RRO feedback signal. In both cases, high value of $\max_\tau C(\tau) \gtrsim 0.4$ distributes same frequency range $0.001 \lesssim \Omega \lesssim 0.03$ under the attractor merging condition ($K = -0.038$ for RRO method, $K = -0.0064$ for DG-RRO method) ($a = 2.82, b = 10, \sigma_{\mathrm{rro}} = 0.6, \sigma_{\mathrm{dg}} = 0.3, A_s = 0.001$).

quently, higher sensitivity was observed under a weak input signal, i.e., a higher degree of synchronization was observed using a weak input signal (Fig. 6).

The conventional RRO feedback signal has been considered for application in biological systems [27], [29]–[31]. We demonstrated that the RRO method may contribute to the minimally invasive light therapy, in which a light stimulus is applied to patients for stabilizing their disturbed circadian rhythms owing to pathological conditions [30]. In the widely used light therapy, the stimulus strength is not optimized for each state of the patient; therefore, a stimulus that is too strong often induces side effects [35]–[37]. Our previous study showed that the stimulus strength may be reduced when the stimulus is planned using the RRO method [30]. Furthermore, the RRO feedback signals can be applied to the biofeedback signals [31] (reviewed in [25]). Therefore, the DG-RRO method, which induces the chaotic resonance using a weaker feedback, might facilitate the application of chaotic resonance in biological systems.

The limitations of this study are discussed as follows. First, we focused on a discrete cubic map; however, the DG-RRO method should be applied to neural systems, where the high-accurate estimation of map function is desired. Although the DG-RRO method does not change the internal parameters of systems and the conventional RRO method, a more detailed map function profile is required to define the feedback signal. One such method involves the stroboscopic phase space portrait and Poincaré sections [38], [39]. Our previous study estimated the map functions using Chua's circuit. Based on the map function profile, the RRO feedback signal was applied to induce the chaotic resonance [32]. This

estimation method might be effective for applying the RRO and DG-RRO methods to actual neural systems. Second, the amount of feedback strength perturbation to induce the attractor-merging bifurcation varies depending on the map function of chaotic systems. Therefore, the advantages of the DG-RRO method must be validated for various types of chaotic maps. Third, several types of noises, such as additive and contaminant noises, must be considered in actual neural systems [40]. Hence, these issues should be evaluated in future studies.

As conclusions, the proposed method may pave the way for utilizing chaotic resonance in engineering scenarios where only stochastic resonance has been applied.

Acknowledgments

Author Contributions

TI, YE, and SN conceived the methods, wrote the main manuscript, and prepared all figures. TI, YE, and SN contributed equally to this study. NW, HD, TY, and HN analyzed and discussed the results. All authors have read and approved the submitted version.

References

[1]   S. Sinha and B.K. Chakrabarti, "Deterministic stochastic resonance in a piecewise linear chaotic map," Phys. Rev. E, vol.58, no.6, p.8009, 1998.

[2]   F. Hadaeghi, M.R. Hashemi Golpayegani, S. Jafari, and G. Murray, "Toward a complex system understanding of bipolar disorder: A chaotic model of abnormal circadian activity rhythms in euthymic bipolar disorder," Australian & New Zealand Journal of Psychiatry, vol.50, no.8, pp.783–792, 2016.

[3]   A. Bayani, F. Hadaeghi, S. Jafari, and G. Murray, "Critical slowing down as an early warning of transitions in episodes of bipolar disorder: A simulation study based on a computational model of circadian activity rhythms," Chronobiology International, vol.34, no.2, pp.235–245, 2017.

[4]   V.S. Anishchenko, V. Astakhov, A. Neiman, T. Vadivasova, and L. Schimansky-Geier, Nonlinear Dynamics of Chaotic and Stochastic Systems: Tutorial and Modern Developments, Springer Science & Business Media, 2007.

[5]   M. Khona and I.R. Fiete, "Attractor and integrator networks in the brain," Nat. Rev. Neurosci., vol.23, pp.744–766, 2022.

[6]   S. Nobukawa and H. Nishimura, "Synchronization of chaos in neural systems," Front. Appl. Math. Stat., vol.6, p.19, 2020.

[7]   R. Benzi, A. Sutera, and A. Vulpiani, "The mechanism of stochastic resonance," J. Phys. A: Math. Gen., vol.14, no.11, p.L453, 1981.

[8]   S. Nobukawa, R. Hashimoto, H. Nishimura, T. Yamanishi, and M. Chiba, "Noise-induced phenomena in the kaldor business cycle model," Transactions of the Institute of Systems, Control and Information Engineers, vol.30, no.12, pp.459–466, 2017.

[9]   S. Nobukawa and H. Nishimura, "Enhancement of spike-timing-dependent plasticity in spiking neural systems with noise," Int. J. Neur. Syst., vol.26, no.05, p.1550040, 2016.

[10]   L. Gammaitoni, P. Hänggi, P. Jung, and F. Marchesoni, "Stochastic

resonance," Rev. Mod. Phys., vol.70, no.1, p.223, 1998.

[11] G.P. Harmer, B.R. Davis, and D. Abbott, "A review of stochastic resonance: Circuits and measurement," IEEE Trans. Instrum. Meas., vol.51, no.2, pp.299–309, 2002.

[12] F. Moss, L.M. Ward, and W.G. Sannita, "Stochastic resonance and sensory information processing: a tutorial and review of application," Clinical Neurophysiology, vol.115, no.2, pp.267–281, 2004.

[13] A. Pikovsky, M. Rosenblum, and J. Kurths, Synchronization: A Universal Concept in Nonlinear Sciences, Cambridge University Press, 2003.

[14] S. Rajasekar and M.A.F. Sanjuán, Nonlinear Resonances, Springer, 2016.

[15] S. Ibáñez, P. Fierens, R. Perazzo, G. Patterson, and D. Grosz, "On the dynamics of a single-bit stochastic-resonance memory device," Eur. Phys. J. B, vol.76, no.1, pp.49–55, 2010.

[16] A. Stotland and M. Di Ventra, "Stochastic memory: Memory enhancement due to noise," Phys. Rev. E, vol.85, no.1, p.011116, 2012.

[17] Y. Tadokoro, H. Tanaka, Y. Nakashima, T. Yamazato, and S. Arai, "Enhancing a BPSK receiver by employing a practical parallel network with stochastic resonance," Nonlinear Theory and its Applications, IEICE, vol.10, no.1, pp.106–114, 2019.

[18] L. Duan, F. Duan, F. Chapeau-Blondeau, and D. Abbott, "Stochastic resonance in Hopfield neural networks for transmitting binary signals," Phys. Lett. A, vol.384, no.6, p.126143, 2020.

[19] Y. Kurita, M. Shinohara, and J. Ueda, "Wearable sensorimotor enhancer for fingertip based on stochastic resonance effect," IEEE Trans. Human-Mach. Syst., vol.43, no.3, pp.333–337, 2013.

[20] L.R. Enders, P. Hur, M.J. Johnson, and N.J. Seo, "Remote vibrotactile noise improves light touch sensation in stroke survivors' fingertips via stochastic resonance," J. NeuroEngineering Rehabil., vol.10, no.1, p.105, 2013.

[21] N.J. Seo, M.L. Kosmopoulos, L.R. Enders, and P. Hur, "Effect of remote sensory noise on hand function post stroke," Front. Hum. Neurosci., vol.8, p.934, 2014.

[22] Y. Kurita, Y. Sueda, T. Ishikawa, M. Hattori, H. Sawada, H. Egi, H. Ohdan, J. Ueda, and T. Tsuji, "Surgical grasping forceps with enhanced sensorimotor capability via the stochastic resonance effect," IEEE/ASME Trans. Mechatronics, vol.21, no.6, pp.2624–2634, 2016.

[23] O. Van der Groen, M.F. Tang, N. Wenderoth, and J.B. Mattingley, "Stochastic resonance enhances the rate of evidence accumulation during combined brain stimulation and perceptual decision-making," PLoS Comput. Biol., vol.14, no.7, p.e1006301, 2018.

[24] H. Nishimura, N. Katada, and K. Aihara, "Coherent response in a chaotic neural network," Neural Processing Letters, vol.12, no.1, pp.49–58, 2000.

[25] S. Nobukawa, H. Nishimura, N. Wagatsuma, K. Inagaki, T. Yamanishi, and T. Takahashi, "Recent trends of controlling chaotic resonance and future perspectives," Front. Appl. Math. Stat., vol.7, p.760568, 2021.

[26] S. Nobukawa, H. Nishimura, T. Yamanishi, and H. Doho, "Controlling chaotic resonance in systems with chaos-chaos intermittency using external feedback," IEICE Trans. Fundamentals, vol.E101-A, no.11, pp.1900–1906, Nov. 2018.

[27] S. Nobukawa, N. Shibata, H. Nishimura, H. Doho, N. Wagatsuma, and T. Yamanishi, "Resonance phenomena controlled by external feedback signals and additive noise in neural systems," Sci. Rep., vol.9, no.1, pp.1–15, 2019.

[28] S. Nobukawa, N. Wagatsuma, and H. Nishimura, "Chaos-chaos intermittency synchronization induced by feedback signals and stochastic noise in coupled chaotic systems," IEICE Trans. Fundamentals, vol.E103-A, no.9, pp.1086–1094, Sept. 2020.

[29] S. Nobukawa and N. Shibata, "Controlling chaotic resonance using external feedback signals in neural systems," Sci. Rep., vol.9, no.1, p.4990, 2019.

[30] H. Doho, S. Nobukawa, H. Nishimura, N. Wagatsuma, and T. Takahashi, "Transition of neural activity from the chaotic bipolar-disorder state to the periodic healthy state using external feedback signals," Front. Comput. Neurosci., vol.14, p.76, 2020.

[31] S. Nobukawa, N. Wagatsuma, H. Nishimura, H. Doho, and T. Takahashi, "An approach for stabilizing abnormal neural activity in ADHD using chaotic resonance," Front. Comput. Neurosci., vol.15, p.76, 2021.

[32] S. Nobukawa, H. Doho, N. Shibata, H. Nishimura, and T. Yamanishi, "Chaos-chaos intermittency synchronization controlled by external feedback signals in Chua's circuits," IEICE Trans. Fundamentals, vol.E103-A, no.1, pp.303–312, Jan. 2020.

[33] S. Nobukawa, N. Wagatsuma, H. Nishimura, K. Inagaki, and T. Yamanishi, "Memory storage systems utilizing chaotic attractor-merging bifurcation," IEEE Access, vol.10, pp.15699–15706, 2022.

[34] T. Iinuma, Y. Ebato, S. Nobukawa, A.T. Tran, N. Wagatsuma, K. Inagaki, H. Doho, T. Yamanishi, and H. Nishimura, "Extremely weak feedback method for controlling chaotic resonance," 2023 IEEE International Conference on Systems, Man, and Cybernetics (SMC), IEEE, 2023.

[35] M. Terman and J.S. Terman, "Light therapy for seasonal and nonseasonal depression: Efficacy, protocol, safety, and side effects," CNS Spectrums, vol.10, no.8, pp.647–663, 2005.

[36] D. Sit, K.L. Wisner, B.H. Hanusa, S. Stull, and M. Terman, "Light therapy for bipolar disorder: A case series in women," Bipolar Disorders, vol.9, no.8, pp.918–927, 2007.

[37] T. Abreu and M. Bragança, "The bipolarity of light and dark: A review on bipolar disorder and circadian cycles," Journal of Affective Disorders, vol.185, pp.219–229, 2015.

[38] S. Nobukawa, H. Nishimura, T. Yamanishi, and J.Q. Liu, "Analysis of chaotic resonance in Izhikevich neuron model," PloS ONE, vol.10, no.9, p.e0138919, 2015.

[39] S. Nobukawa, H. Nishimura, and T. Yamanishi, "Chaotic resonance in typical routes to chaos in the Izhikevich neuron model," Sci. Rep., vol.7, no.1, pp.1–9, 2017.

[40] S. Nobukawa, N. Wagatsuma, H. Nishimura, K. Inagaki, and T. Yamanishi, "Influence of additive and contaminant noise on control-feedback induced chaotic resonance in excitatory-inhibitory neural systems," IEICE Trans. Fundamentals, vol.E106-A, no.1, pp.11–22, Jan. 2023.

Takahiro Iinuma graduated from the Department of Computer Science, Chiba Institute of Technology in 2022. He is a student in Graduate School of Information and Computer Science, Chiba Institute of Technology. His research interest includes the functionality of chaotic dynamics. He is a member of IEEE, SICE, and IEICE. He was awarded the Best Paper Award of SSI in 2021.

Yudai Ebato graduated from the Department of Computer Science, Chiba Institute of Technology in 2022. He is a student in Graduate School of Information and Computer Science, Chiba Institute of Technology. His research interest includes the functionality of chaotic dynamics. He is a member of IEEE and SICE.

Sou Nobukawa graduated from the Department of Physics and Earth Sciences, University of Ryukyus, in 2006, completed his doctoral program at the University of Hyogo and received his Ph.D. degree in 2013. He is a professor in the Department of Computer Science, Chiba Institute of Technology. His research interests include chaos/bifurcation and neural networks. He is a member of IEEE, INNS, JNNS, IEICE, SICE, ISCIE, and others. He was awarded the SICE Encouragement Prize in 2016; the Young Researcher Award by the IEEE Computational Intelligence Society, Japan Chapter; the Best Paper Award at the 29th Symposium on Fuzzy, Artificial Intelligence, Neural Networks and Computational Intelligence in 2019; the Excellent Research Award by the Japanese Neural Network Society/the Best Paper Award of SSI in 2021; and Best Paper Award of FIT in 2022.

Nobuhiko Wagatsuma received his B.S., M.S., and Ph.D. degrees from the University of Tsukuba in 2004, 2006, and 2009, respectively. He is currently a lecturer at the Faculty of Science, Department of Information Science, Toho University. His research interests include visual attention and computational neuroscience.

Keiichiro Inagaki received his Ph.D. degree in Engineering from Chubu University in 2007. During 2007–2009, he was a postdoctoral researcher at the Washington University School of Medicine in St. Louis, Department of Anatomy and Neurophysiology as well as the Department of Otolaryngology. During 2009–2013, he was a postdoctoral researcher at RIKEN. In 2013, he joined the Department of Robotic Science and Technology, Chubu University, where he worked as an assistant professor and a senior assistant professor in 2014–2021; he currently works as an associate professor. He is a member of IEEE, IEICE, JNNS, JNS, and SFNs. He was awarded the Best Excellent Research Award by the Japanese Neural Network Society in 2017.

Hirotaka Doho graduated from the Faculty of School Education, Hiroshima University, in 1985, completed the Master's program at Hyogo University of Teacher Education, receiving a Master's degree in 2000. He received his Ph.D. degree from the University of Hyogo in 2022. He is a Professor in the Faculty of Education, Kochi University. His research interests include nonlinear dynamics of neural networks.

Teruya Yamanishi received his MS degree in science education from Kobe University in 1991, and a PhD degree in physics from Kobe University in 1994. He is a professor at the Osaka Seikei University, where he studies mathematical information science for the brain and develops tools for utilizing biometric data.

Haruhiko Nishimura graduated from the Department of Physics, Shizuoka University in 1980 and completed his doctoral program at Kobe University in 1985. He is currently a Professor in the Faculty of Informatics, Yamato University and an emeritus professor in the Graduate School of Applied Informatics, University of Hyogo. His research interests include intelligent systems science based on several architectures, such as neural networks and complex systems. He is also a researcher in biomedical, healthcare, and high-confidence sciences. He is a member of IEEE, IEICE, IPSJ, JNNS, and other organizations, and was awarded the ISCIE paper prize in 2001 and the JSKE paper prize in 2010 and 2022.